In vivo Raman flow cytometry for real-time detection of carbon nanotube kinetics in lymph, blood, and tissues

Alexandru S. Biris
University of Arkansas at Little Rock
Applied Science Department
Nanotechnology Center
Little Rock, Arkansas 72204

Ekaterina I. Galanzha
University of Arkansas for Medical Sciences
Philips Classic Laser and Nanomedicine Laboratories
Little Rock, Arkansas 72205

Zhongrui Li
Meena Mahmood
Yang Xu
University of Arkansas at Little Rock
Applied Science Department
Nanotechnology Center
Little Rock, Arkansas 72204

Vladimir P. Zharov
University of Arkansas for Medical Sciences
Philips Classic Laser and Nanomedicine Laboratories
Little Rock, Arkansas 72205

Abstract. Nanoparticles are intensively being explored as contrast agents for medical diagnostics and therapies using various optical methods. We present the first demonstration of the use of time-resolved Raman spectroscopy for *in vivo* real-time detection of circulating carbon nanotubes (CNTs) or cancer cells labeled with CNTs in the lymph, blood, and tissues of live animals with fast spectral acquisition times of down to few milliseconds. After intravenously administering CNTs in the tail vein of the rat, this technique provides the ability to detect the circulation of CNTs in the blood microvessels of the intact rat ear. The capability of Raman spectroscopy is also demonstrated to monitor, identify, and image the CNTs during their transportation by lymphatics in the rat ear and mesentery. The strong and specific Raman scattering properties of CNTs make it possible to detect *in vitro* and *in vivo* single cancer cells (HeLa) tagged with CNTs. *In vivo* Raman flow cytometry opens a new avenue for multiparameter analysis of circulating nanoparticles with strong Raman scattering properties and their pharmokinetics in blood and lymph systems. Moreover, this technology has the potential for molecular detection and identification of circulating tumor cells, and infections labeled with CNTs.
[DOI: 10.1117/1.3119145]

Keywords: *In vivo* flow cytometry; Raman spectroscopy; carbon nanotubes; cancer cells; blood and lymph flow.

Paper 08276RR received Aug. 8, 2008; revised manuscript received Feb. 11, 2009; accepted for publication Feb. 15, 2009; published online Apr. 28, 2009.

1 Introduction

Carbon nanotubes (CNTs) with unique, well-controlled chemical, physical, electronic, and mechanical properties exhibit great potential in biology and medicine in areas such as gene/drug delivery, bacterial filters, molecular diagnoses, and cancer and infection treatments.[1–12] Before any clinical applications of CNTs can be practical, it is imperative to determine the critical *in vivo* parameters, namely, pharmacological profiles such as the CNT clearance rate from the blood circulation and their dynamic distribution in tissues and organs.[13–16] The first CNT-related studies were performed *ex vivo* in static conditions using blood sampling and radioactive or near-infrared (NIR) fluorescence techniques.[12–14] The high NIR absorption of CNTs provided the opportunity to use them as excellent photoacoustic (PA) contrast agents for the detection of circulating cells and pathogens as well as tumor imaging.[17–19] As an alternative, Raman spectroscopy has been applied to monitor the CNTs *in vivo* in static condition, demonstrating large signal-to-noise ratios (SNRs) and molecular specificity due to the strong Raman scattering signals from CNTs and their specific vibrational spectra fingerprints, respectively.[20–25] Raman spectroscopy was successfully used also in *in vitro* flow cytometry using surface-enhanced Raman scattering (SERS) nanoparticles.[26] However, the application of Raman flow cytometry (RFC) for *in vivo* studies, especially for single cell detection, has not been reported. Here, we demonstrate the ability of CNTs to serve as excellent *in vivo* Raman contrast agents, resulting in a time-resolved measurement of the CNTs kinetics in blood and lymphatics, as well as selective detection of single cancer cells in small animal models. In particular, this paper presents the successful use of the *in vivo* RFC approach in two various applications: (1) *in vivo* real-time detection of single-walled CNT clearance in lymph and blood flow and (2) detection of single cancer cells labeled with CNTs in biological tissues.

2 Materials and Methods

2.1 *CNT Preparation*

Single-walled CNTs were grown by radio-frequency chemical vapor deposition (rf-CVD) on a Fe:Mo/MgO catalyst with methane as the carbon source and processed, as described

Address all correspondence to: Alexandru S. Biris, PhD, Nanotechnology Center, Applied Science Department, University of Arkansas at Little Rock, AR, 72204. E-mail: asbiris@ualr.edu and Vladimir P. Zharov, PhD, DSc, Philips Classic Laser Laboratories, University of Arkansas for Medical Sciences, Little Rock, AR 72205. E-mail: zharovvladimirp@uams.edu.

1083-3668/2009/14(2)/021006/10/$25.00 © 2009 SPIE

previously.[27] The individually dispersed CNT solution was obtained by wrapping double stranded DNA around the nanotubes, an approach that was used previously[1] to individually disperse CNTs in liquid solutions. Salmon double-stranded deoxyribonucleic acid (dsDNA) purchased from Sigma-Aldrich was introduced in the buffer solution (10 mM, pH =7.3) at a concentration of 0.7 mg/mL. Then 0.4 mg of CNTs were added into 5 mL of dsDNA buffer solution followed by a strong sonication over a water-ice bath (Branson Model 1510R-MT, 42 kHz, output power 70 W) for 1 h. The resulting solution was centrifuged for 15 h at 16,000*g* to remove the undispersed CNTs. The result was a uniformly darker solution with no visible agglomerations of CNTs. This approach can be used as a preliminary step toward the complete bioconjugation of CNTs to antibodies and folates for controlled delivery of CNTs to tumors.

2.2 *CNTs Characterization*

The CNT physical characteristics after their synthesis were assessed using several analytical techniques that included microscopy, spectroscopy, and thermogravimetric analysis.

2.2.1 *Atomic force and transmission electron microscopy*

The CNT length analysis and their individual dispersion were studied by atomic force microscopy (Veeco Multimode Scanning Probe Microscope with Nanoscope IIIa Controller; Veeco Instruments, Woodbury, New York) and transmission electron microscopy (TEM) using a JEOL 2100 FE electron microscope (JEOL-USA, Peabody, Massachusetts). For TEM analysis, the CNTs were deposited onto carbon-coated copper grids without staining to reduce the possibility of artifacts.

2.2.2 *Epifluorescence and light microscopy*

Phase-contrast and transmittance microscopy was performed using a light microscope (Axioskop 2 Plus, Carl Zeiss, Inc., Germany) equipped with a 12-bit Color MicroImager II Cooled digital camera (QImaging, Burnaby, Canada) with a resolution of 1.3 million pixels. The 100× or 63× oil immersion objectives (Carl Zeiss) were used to visualize and acquire the images and their sequences with a digital image and video recording software, StreamPix (Norpix, Inc., Montreal, Canada). The light microscopy system was additionally equipped with a filter set (FITC, Carl Zeiss) consisting of a bandpass filter covering 450 to 490 nm for an exciter and an absorbance filter covering a wavelength of 515 nm to acquire epifluorescence images for the live (green fluorescent) and dead (red fluorescent) cells (see later). Fluorescent dye—FITC-dextran 150,000 (Sigma Chemicals)—was used for the visualization of lymphatics and verification of Raman data.

2.3 *Confocal Raman Microscope/Spectrometer*

For the *in vitro* and *in vivo* experiments, three lasers in continuous wave (cw) mode were alternatively used for the excitation of Raman spectra: (1) aurgon laser with a wavelength of 514 nm and power from 2 to 99 mW; (2) a He-Ne laser with a wavelength of 633 nm and power from 5 to 20 mW; and (3) a diode laser with a wavelength of 785 nm and power from 5 to 99 mW. The scattered light was collected in the back-scattering geometry by a confocal Raman microscope on an Olympus BX-51 platform, with 10, 50, and 100× microobjectives. These microobjectives were simultaneously used to focus the incident beam onto the sample. The adjustable laser circular beam size ranged from 1 to 10 μm. An automated stage provided 3-D (*X-Y-Z*) spatial scanning with a step size of 1 μm. Raman scattering spectra were obtained with a Raman spectrometer (Horiba Jobin Yvon LabRam HR800) with 1800- and 600-lines/mm gratings equipped and a Peltier-cooled CCD camera. The spectral resolution was below 0.3 cm^{-1}, and in most experiments the collected signal for each data point was the average of 10 measurements. Raman spectra were calibrated with a standard silicon wafer using a specific peak of 520 cm^{-1}, corresponding to the Si-Si stretching band.

2.4 *Cell Cultures*

For the primary culture the frozen cells (Human Cervical cancer HeLa Cells) were thawed and seeded in 75-mm^2 flasks at a density of 1×10^6 cells, harvested under minimum essential medium (MEM), and supplemented by 10% FBS, 1% PS, and 1% glutamic acids (nonessential amino acid). The cells were cultured at 37 °C and 5% CO_2 for several days to grow and develop, while the medium was changed every second day. After the medium was carefully removed, the cells were treated with 1× trypsin in phosphate-buffered saline (PBS) and incubated for 10 min for detachment followed by centrifugation at 1100 rpm for 10 min. The supernatant was removed and the cells were resuspended into a fresh medium with dsDNA-wrapped CNTs. The CNT concentration was adjusted based on the desired experimental design, as presented. After the administration of CNTs, the cells were incubated in 75-mm^2 flasks with the CNT solution for 12, 24, and 48 h under identical conditions before the cells were used for experiments. For the cytotoxic studies, the cells were trypsinized and cultured in 35-mm culture plates (1×10^5 cells/plate) with different concentrations of single-walled CNTs for 48 h under identical conditions. Standard ethedium bromide (EB) and acridine orange staining kits (1 part of EB in PBS: 1 part of 100 mg/ml of acridine orange in PBS) were used to detect and analyze the number of dead cells. At least 300 cells were examined under the fluorescent microscopic camera with a 10× objective. Acridine orange is a commonly used dye, which stains the live cells green while the dead cells are stained brown by the EB. To observe the cytotoxic effects of the CNTs only, all the cell viability results were normalized.

A one-way analysis of variance (ANOVA) was used for the statistical analyses of the percentage of the dead cells; *P* values of 0.05 or less were considered to indicate significance.

2.5 *Animal Model*

The feasibility studies of *in vivo* RFC involved male Fisher (F344) rat models at ~4 weeks of age weighing 150 to 180 g. The protocol was approved by the Institutional Animal Care and Use Committee (IACUC) of the University of Arkansas for Medical Sciences (UAMS). The rat mesentery was used for proof of concept *in vivo* RFC because it consists of a very thin (7- to 15-μm) transparent connective tissue with a single layer of blood and lymph microvessels.[28] After administering standard anesthesia [ketamine/xylazine, 50/10 mg/kg, intramusculor (im)] the rats were laparoto-

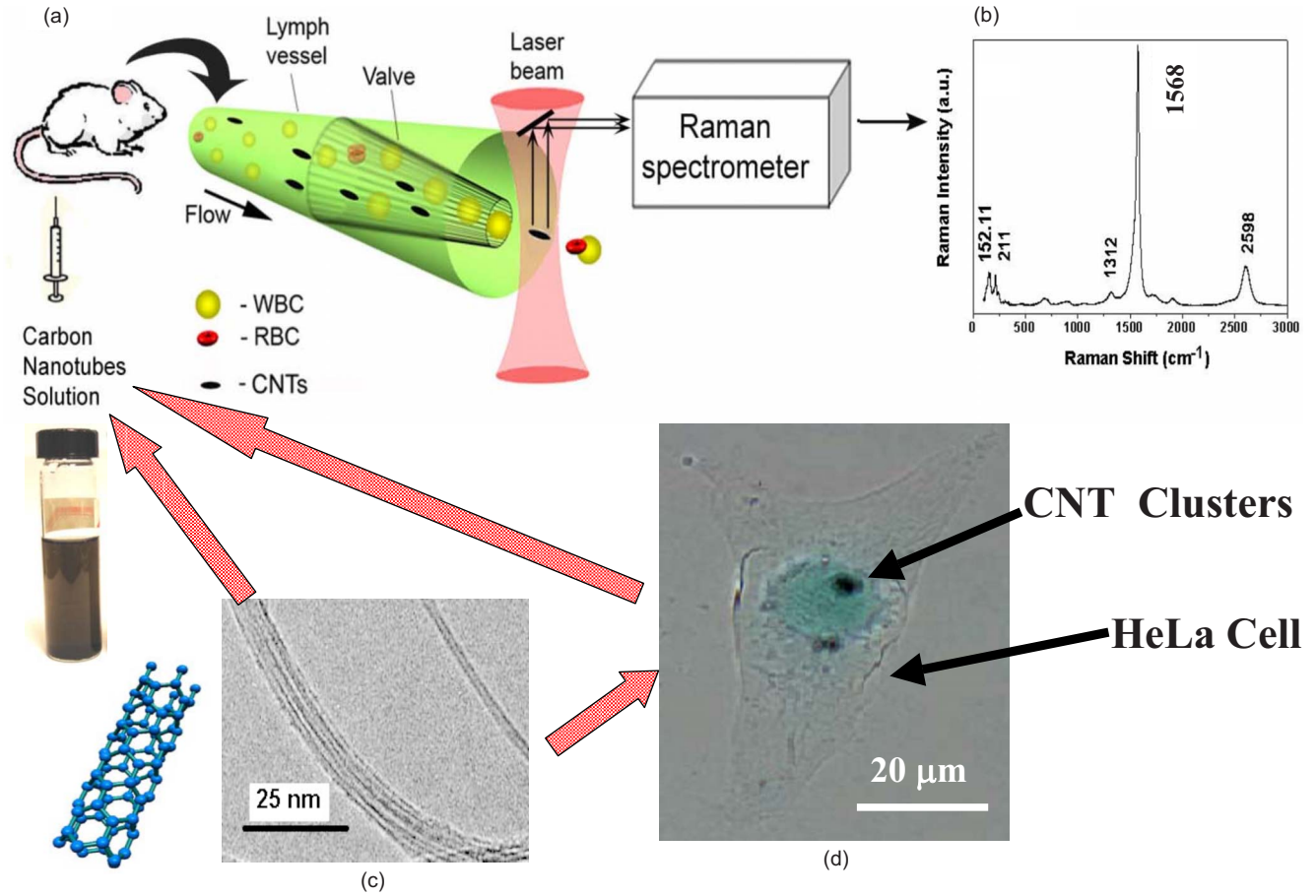

Fig. 1 (a) Schematic of the *in vivo* RFC for real-time monitoring of carbon nanotube biodistribution in a complex biological environment (e.g., in lymphatics) based on their strong Raman scattering and unique Raman spectra (b). (c) The spatial structure (left) and TEM image (right) of carbon nanotubes with diameters ranging between 1 and 2 nm; these nanoparticles in PBS solution were injected intravenously in the bloodstream or in skin. (d) Human cervical cancer HeLa cells were incubated with carbon nanotubes and injected in lymphatics or ear skin.

mized by a midabdominal incision. Immediately after exposure, the mesentery was placed on a customized and heated (37.7 °C) module fixed on the automated stage of the Olympus microscope. The mesentery was suffused with warmed Ringer's solution (37 °C, pH 7.4) containing 1% BSA to prevent protein loss. Besides mesentery, the vasculature was also examined in the intact rat ear. We studied the ear blood vessels were located 50 to 150 μm deep and had diameters in the range of 30 to 50 μm and blood velocities of 1 to 5 mm/sec. Lymph microvessels under study had a similar depth and 150 to 200 μm diameters with average lymph flow velocity in the range of 0.1 to 0.5 mm/s. The laser radiation was focused either on the interstitial ear tissue, blood or lymph ear microvessels, or in the mesentery vessels, depending on the experiment performed. The CNT solution was delivered with a 28 gauge needle inserted intravenously in the rat tail vein or by local subcutaneous injection in the ear tissue. Additionally, cancer cells with CNTs were administered locally in the rat mesentery or injected in the ear tissue on areas close to lymph vessels.

2.6 *Temperature Measurements*

The thermal analysis was performed using a calibrated forward-looking IR (FLIR) Thermacam SC500 thermal camera (FLIR Systems, Inc., Boston, Massashusetts). The thermal images were acquired at 1 Hz and recorded to a sequence file. The camera lens used has a field of view (FOV) of approximately 4×6 mm with a maximum resolution of 18 μm/pixel. Images were recorded prior to and during the laser exposure of tissue.

3 Results

3.1 *Carbon Nanotube Characterizations*

Figure 1(a) shows experimental schematics of *in vivo* RFC using CNTs as Raman contrast agents with unique Raman scattering spectrum [Fig. 1(b)]. The CNTs were individually dispersed into a solution [Fig. 1(c)] that was injected either into the rat tail vein or skin. Their biodistribution analysis was done based on the intensity of their corresponding Raman peaks. Additionally, HeLa cells were loaded with the CNTs using endocytosis, and injected in tissue followed by their imaging with the Raman spectroscopy technique.

The average length and diameter of single-walled CNTs used in this study [Fig. 1(c)] were 150 to 190 nm and 1.5 to 1.8 nm, respectively. The Raman spectra of these CNTs contain characteristic bands in two spectral regions: so-called radial breathing modes (100 to 500 cm^{-1}), which

strongly depend on the diameters and chirality of the nanotubes,[22,23] and a high-wave-number region (tangential and longitudinal modes) between 1200 and 3000 cm^{-1} [Fig. 1(b)]. The D band, positioned between 1250 and 1450 cm^{-1}, is associated with vacancies and the presence of other carbonaceous impurities (amorphous carbon, glassy carbon, etc) that destroy the graphitic symmetry. Band G (between 1500 and 1600 cm^{-1}) corresponds to the splitting of the E_{2g} stretching mode for graphite. The 2-D band (between 2450 and 2650 cm^{-1}), which is the second-order harmonic of the D band, is associated with the degree of crystallinity of the graphitic layers.[21–23] The G band has the highest intensity (and referred to as Raman signals) and therefore it was further used to dynamically evaluate the presence of CNTs in the biological environments *in vivo*.

3.2 *Comparison of Excitation Wavelengths*

Initial experiments using *in vivo* optical imaging and *ex vivo* immunochemistry assays revealed that laser radiations of 633 and 785 nm wavelengths at power levels of less than 20 mW did not produce any visible tissue and vessel photodamage. Laser radiation at 514 nm at the same power was found to induce lymph vessel constrictions and local tissue damages. In addition, higher blood absorption of the 514-nm laser radiation, compared to that of 633 or 785 nm, may restrict its application for studying tissues with rich blood networks. Raman signals collected with the 514-, 633-, and 785-nm laser radiations were found to be comparable in intensity (slightly higher for the 633-nm excitation), while the background signal levels were found to decrease as the excitation wavelength increased (Fig. 2). Thus, the laser radiations of 633 nm and especially 785 nm are the most promising for the CNTs *in vivo* detection since the background signals of the surrounding tissues have minimum absorption levels in the NIR spectral range.[25] Temperature measurements of a 10-ml CNT solution (0.2 mg/mL) irradiated separately for 1 min with each of the three laser wavelengths (514, 633, and 785 nm) revealed a 4 to 5 °C temperature increase when exposed to the 785-nm laser when compared to lower temperature variations (less than 1 °C) for the 514- and 633-nm lasers. These results indicate a higher optical absorption, and hence, heating of CNTs when irradiated with the 785-nm laser, compared to when exposed to the 514- and 633-nm laser radiations. In this paper, a laser wavelength of 633 nm was selected as a reasonable compromise between Raman signal levels (strong enough for CNT detection), minimal thermal effects, and laser penetration into the tissue of a few millimeters, which is sufficient for the Raman assessment of peripheral vessels.

3.2.1 *In vitro identification of HeLa cancer cells labeled with CNTs among red blood cells*

The increase of the incubation time (12, 24, to 48 h) of human cervical HeLa cells with the DNA-wrapped single-walled CNTs led to a gradual enhancement of the Raman signal intensity collected from areas inside the cells [Fig. 3(a)]. These data indicate an increased CNT concentration and number of CNT clusters inside the cells, which were present mostly around the nucleus membrane [Fig. 3(a)]. These results indicate a high accumulation of CNTs both in the cell cytoplasm and inside the nucleus, especially, at increased incubation times. The CNT translocation *in vitro* into cells most probably happened due to endocytosis and other complex processes such as diffusion through transmembrane channels, or adhesive interactions. Some of the most important factors that are responsible for the uptake of CNTs by the cancer cells include their size, surface charge, concentration, temperature, and the biochemical conditions of the delivery.[1] CNT structural characteristics such as the diameter and length are the parameters responsible for their penetration into the cells since they present a snaking behavior when they cross the intracellular membranes. In our study, surprisingly, the CNTs were found to aggregate around the membrane of the nucleus and then penetrate the nuclear membrane into the nucleus after being dispersed individually in the medium solution that was used to feed the HeLa cells. The significant enhancement of the Raman signals from the CNT aggregates present inside the cells provides a direct path for highly sensitive Raman detection of these cells in different biological environments. This is analogous to the synergistic amplification of the PA and photothermal (PT) effects due to the self-assembled nanoclusters inside the living systems.[2] Figure 3(b) at the bottom shows the capability of Raman spectroscopy to simultaneously detect and identify (using the specific CNT G band spectral position) a single HeLa cell with CNTs (48-h incubation) in a monolayer of red blood cells (RBCs) from a rat. The results were obtained *in vitro* by spatially scanning the laser beam across the sample with a velocity of 0.01 mm/s and "spectral" scanning (i.e., collection of a 1200- to 1800-cm^{-1} Raman spectral window) at a 50-ms acquisition time. Significant high SNRs and low background signal levels of the RBCs also enabled us to distinguish one cancer cell among hundreds of RBCs in a concentrated blood sample 120 μm thick (not shown here).

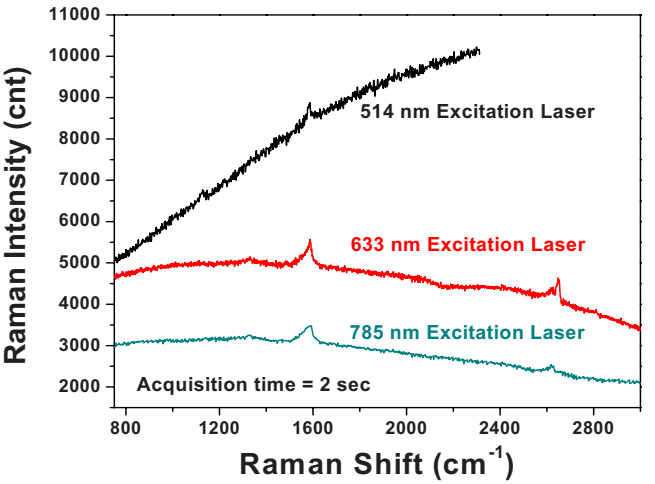

Fig. 2 Raman spectra of the ear tissue with locally injected CNTs that were collected with various laser wavelengths.

3.2.2 *In vivo detection of the carbon nanotubes distribution in rat ear tissue*

To further estimate the *in vivo* maximal achievable sensitivity of the technique in almost ideal static conditions, a small amount of CNT solution (10 μl, concentration of 0.2 mg/ml) was locally injected under the skin of the rat ear in an area

free of blood microvessels. The high-resolution (40×) transmission imaging of the ear tissue was used to visualize the location of the blood vessels as well as the lymphatic vessels networks highlighted by a local administration of conventional Evans Blue dye[28] [Fig. 4(a)]. The optical monitoring of this area revealed that the initially highly localized CNTs [Fig. 4(b), arrow] evolved into an elongated zone about 20 min after delivery [Fig. 4(c), arrow].

The collection of specific Raman spectra of the CNT-free ear tissue (e.g., before the CNT injection) required relatively long acquisition times because of the relatively low intensity of Raman signals. As an example, Fig. 4(d) shows representative Raman spectra (out of over 50) of the tissue collected *in vivo* at 30-, 40-, 50-, and 60-s acquisition times. Figure 4(d) indicates that even for relatively long acquisition times (over 60 s) the Raman spectra of the biological tissues did not show any peak at 1568 cm^{-1} [therefore specific only to CNTs—Fig. 1(b)] among the distinctive spectral features of the tissues.

One minute after the CNTs administration, the Raman signal started being collected from the tissue area with the maximum concentration of CNTs [Fig. 4(b)] at different acquisition time intervals and different wavelengths. The 1568-cm^{-1}, CNT-specific peak was visible among the background Raman signals from the ear tissue even for acquisition times of as low as a few dozens milliseconds [Fig. 4(e)]. When the acquisition time was increased, the 1568-cm^{-1} peak became better defined and increased in intensity. At a 2-s acquisition time, besides the G band, the nanotubes' D band (1312 cm^{-1}) also became evident in the Raman spectra [Fig. 4(e)]. These data clearly indicate the difference in the Raman scattering properties of CNTs and biological tissues, especially for short acquisition time intervals (<5 s) when there is a smooth background from tissue with no distinguished Raman spectral features [Fig. 4(e), bottom]. Note that the increase of the 1568-cm^{-1} peak intensity was not accompanied by a similar enhancement of the background signal collected from the surrounding tissue, thus leading to the enhancement of the SNR. Time-related Raman spectral monitoring of the ear tissue (with the acquisition time of 2 s) in an area close to the initial spot of high CNT concentration [see arrow in Figs. 4(b) and 4(c)] and with the starting analysis time of 10 min after CNT injection, demonstrated a gradual enhancement of the 1568-cm^{-1} peak intensity, indicating a continuous concentration increase of CNTs at the point of analysis due to their bioredistribution [Fig. 4(f)].

Taking into account a previous lymphatic study,[28] the obtained kinetic data strongly suggested that CNTs, after their migration into the tissue, were absorbed by the neighboring lymph vessels, followed by their further propagation by the lymphatics. Indeed, regular CNT tissue diffusion usually results in a relatively homogeneous CNT distribution around the injected area, while both the optical images and Raman analysis indicated a significant increase of CNT concentration in one dominant direction, which is likely associated with the lymph microvessels located in the area of CNT injection [Fig. 4(a)].

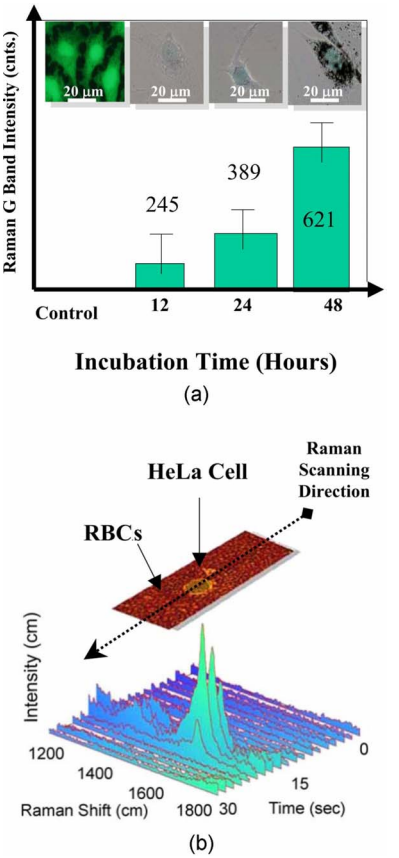

Fig. 3 (a)*In vitro* Raman signals (bottom) (633-nm laser excitation, 20-mW power, and an acquisition time of 50 ms) from single He-La cells in culture petri dishes incubated for 12, 24 and 48 h with CNTs (top). (b) *In vitro* Raman spectra (bottom) of single He-La cells after 48 h incubation with CNTs that was introduced among a monolayer of red blood cells. (RBCs) (top); these data were obtained simultaneously by a fast spectral analysis with an acquisition time of 50 ms and relatively slow laser spatial scanning at a rate of 0.01 mm/s.

3.2.3 *In vivo Raman detection of circulating carbon nanotubes in rat ear blood vessels*

To determine the clearance rate of CNTs, the 100-μl PBS suspension of CNTs (0.2 mg/ml) was injected into the rat blood circulation through the tail vein followed by real-time monitoring of circulating CNTs in a 50 to 70-μm blood ear vessels [Fig. 4(g)] at fixed wavelength near the CNT G band (1568 cm^{-1}). The Raman signals quickly appeared within the first minutes, providing slightly fluctuated continuous background with the average Raman signal amplitudes exceeding 5 to 10 times the Raman background signals from blood vessels. Simultaneously, stronger but less frequent Raman signals were observed above relatively stable Raman backgrounds from CNTs. As discussed before,[17] these phenomena can be associated with the random fluctuations of the CNTs number in the detected volume (i.e., within the focal volume of the excitation laser beam) or appearance of small CNT aggregates. This study revealed the average clearance time of the CNTs from the rat ear microcirculation to be in the range of 20 to 30 min, depending on the quantity of solution and presence of CNT aggregates. No Raman signals of the 1568-cm^{-1} peak were observed 30 to 40 min after injection. The ob-

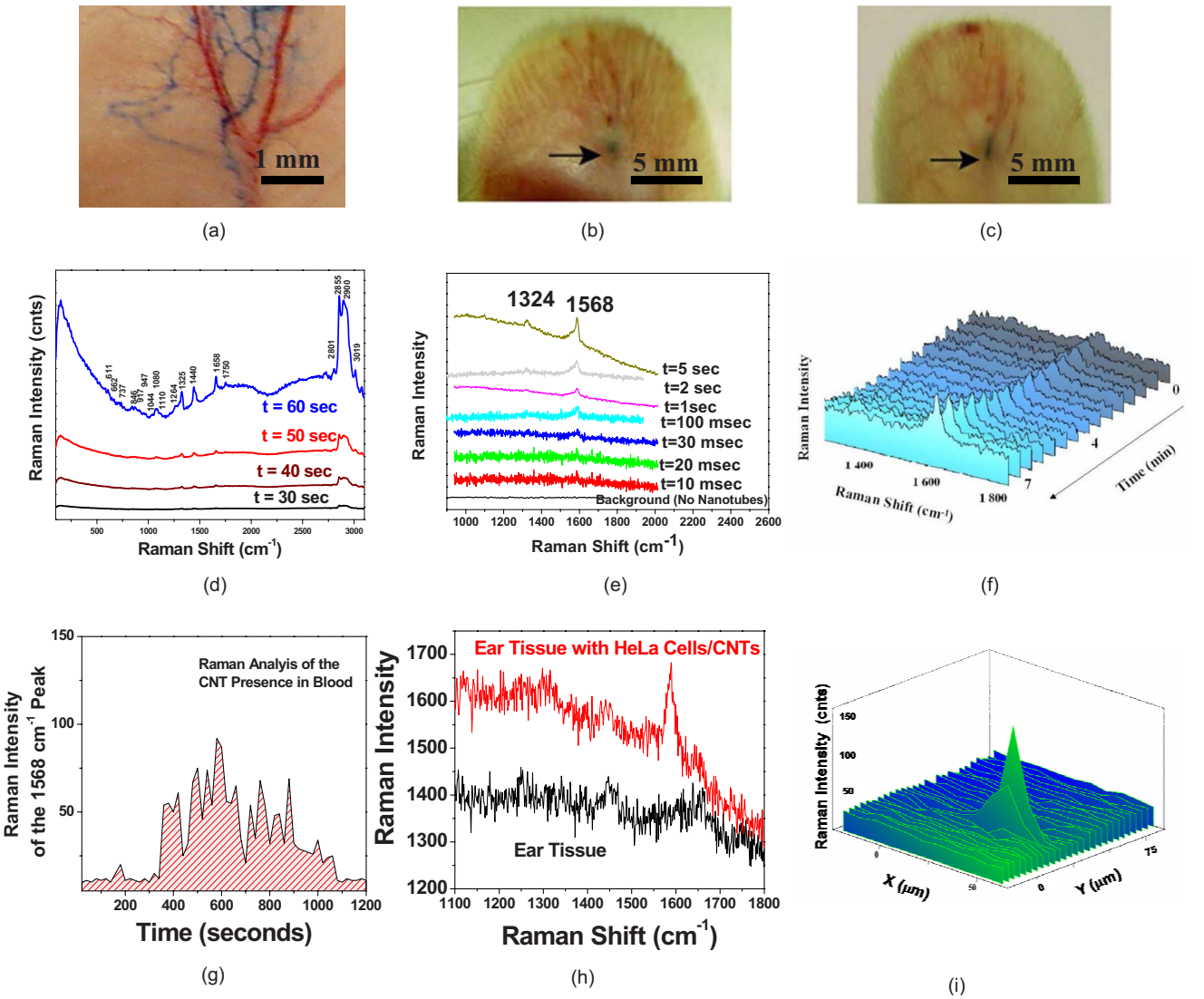

Fig. 4 Optical transmission images of the local area of small animal's ear tissue after the administration of Evans blue dye (a) and in another set experiment at 10 (b) and 20 (c) min after CNT injections only. The arrows in (b) and (c) show the distribution pattern of the CNTs as a function of time. (d) Raman spectra of rat ear tissue areas without CNTs as a function of the Raman spectrum acquisition time, (e) Raman spectra of the rat ear tissue area with CNTs as a function of the Raman acquisition time, and (f) Raman spectra of CNT distribution in the rat ear tissue at area below the injected site as a function time at the Raman acquisition time of 2 s; the time $T=0$ s is the starting time for spectra collection (approximately 10 min after CNT injection). (g) Real-time Raman detection of circulating CNTs in the blood ear microvessels as a function of time after the CNT injection in the tail vein, (h) Raman spectra collected from single He-La cell injected in the ear tissue compared to the Raman background before the cell administration, and (i) 2-D Raman mapping imaging of a single HeLa cancer cells with CNTs in rat ear tissue, based on the CNTs G band intensity spatial variation. All the Raman experiments were performed with the 633-nm laser excitation (20-mw power).

served CNT clearance rate was found to be in a reasonable correlation with the values obtained when using fluorescent and radioactive labels *ex vivo*.[13,14]

3.2.4 *In vivo detection of cancer cells tagged with carbon nanotubes in rat ear tissue*

Next we investigated the potential of RFC to detect cancer cells *in vivo*. HeLa cells were incubated with CNTs for 48 h and injected in a similar manner as the CNTs in the rat ear tissue followed by Raman spectral and spatial scanning (633-nm laser excitation, 20-mW power, 0.5-s acquisition time) of the tissue near the injection site. The characteristic peaks of the CNTs are evident in the spectrum (with an intensity of around 150 counts) above background signals obtained before the administration of cells [Fig. 4(h)]. This high SNR enabled the collection of an *X-Y* Raman map based on the *X-Y* variation of the 1568-cm^{-1} peak intensity. The localized Raman signal 2-D distribution presented in Fig. 4(i) corresponds to the presence of only a single HeLa cell in the ear tissue as verified by (1) low concentration of the injected cells, (2) signal counting from individual cells before injections [Fig. 3(a) and 3], comparability of signal dimension localization with single cell size (~30 μm).

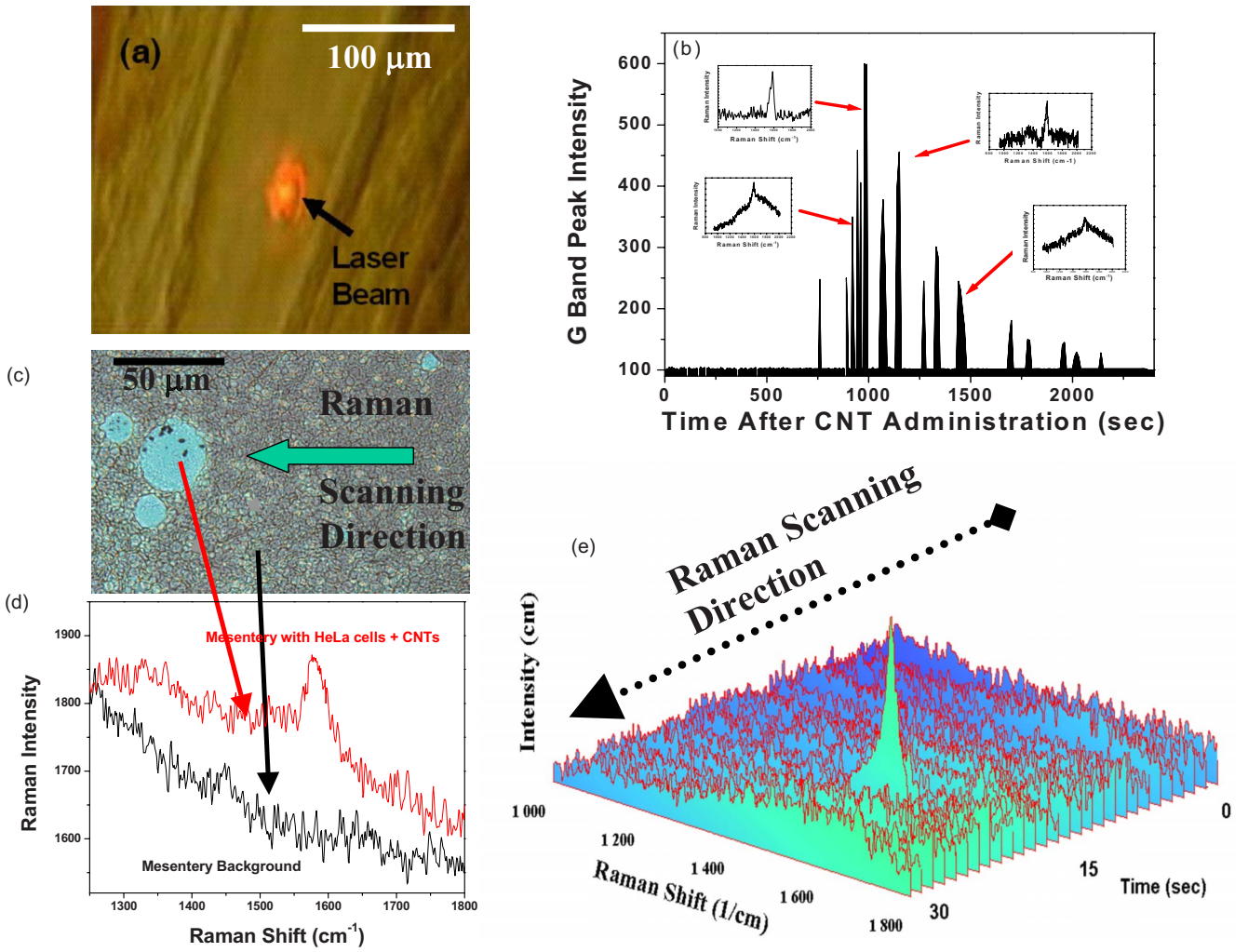

Fig. 5 Optical images of the rat mesentery with the 633-nm laser beam in lymph vessels (diffused due to light scattering phenomena); (b) the intensity of the 1568-cm^{-1} peak (G band) from a lymph vessel as a function of time after CNTs administration; the time $T=0$ s is considered the time of CNTs delivery in mesentery, the insets represent the actual experimental data collected at the respective time intervals and which were provided for comparison of the G band intensity; (c) optical transmission image of one large and two small cancer (HeLa) cells in mesentery (the left side of the image), small black spots inside cells are CNT clusters; (d) Raman spectra from single HeLa cancer cells with CNTs (red) and the Raman spectrum of the background mesenteric tissue (black); and (e) 2-D temporal-spectral imaging of single cancer cell into the mesentery. (Color online only.)

3.2.5 *In vivo Raman detection of carbon nanotubes and cancer cells in rat mesentery lymphatics*

To further verify the previously presented finding of CNT uptaking by lymphatics, the CNT solution (0.05 mg/ml, 100 μl) was topically administered onto the rat mesentery—a thin and relatively transparent structure with clearly distinguished individual 100 to 200-μm-diam lymph vessels [Fig. 5(a)], placed on a heated microscope stage and bathed in warm Ringer's solution 37 °C, pH 7.4). The laser beam was focused onto the area behind the lymph valve [Fig. 1(a)], which acts as a natural nozzle, concentrating the flowing CNTs near the vessel axis.[18] Similar to the CNT blood flow experiments [Fig. 4(g)], time-resolved Raman monitoring of lymphatics was performed by analyzing the 1568-cm^{-1} peak intensity, which is in direct relationship with the number of CNTs present in the focal volume of the laser beam. Taking into consideration the laser scattering phenomena in tissue, this volume was estimated to be approximately 20 to 30 μm^3.

As shown in Fig. 5(b), the time required for the peak at 1568 cm^{-1} to become present in the Raman spectra of the lymph vessel (i.e., time scale of most CNTs uptaking by lymphatics) at an acquisition time of 50 ms was approximately 3–5 min after the local administration of the CNTs. To avoid background Raman signals due to the CNTs possibly present on the mesentery surface, the surface of the area exposed to the laser radiation was continuously washed with warm Ringer's solution. This procedure did not influence the Raman signal levels, suggesting the presence of CNTs only inside the lymph vessels. Raman data indicated that the intensity of the G band gradually increased with the measurement time, which showed a continuous enhancement of the CNT concentration in the lymph vessels due to the CNTs uptaking from the surrounding interstitial tissue. After 15 min, the CNT con-

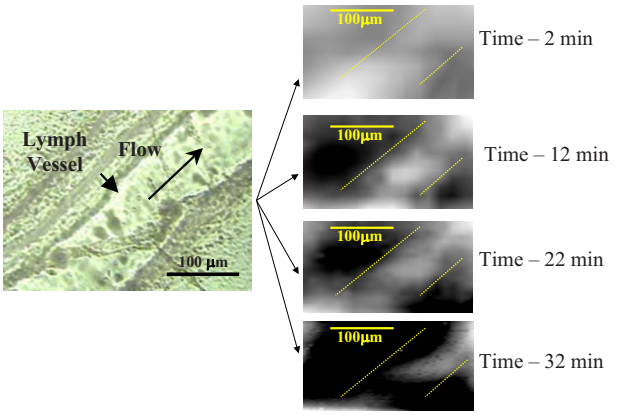

Fig. 6 Optical (left) and Raman *X-Y* mapping images (right) of local area of rat mesentery at 2, 12, 22, and 32 min after CNT injection. The Raman scattering data were collected at regular time intervals of 50 ms/spectra and an excitation wavelength of 633 nm. The laser power was kept constant at 20 mW.

centration inside the lymph vessel was found to decrease, as indicated by Fig. 5(b). CNT-specific Raman signals were detected even beyond 35 min after the initial administration, but were of a significantly lower intensity.

Identical experiments were repeated by the administration of HeLa cells tagged with CNTs (48-h incubation time) onto the mesentery. The presence of HeLa cells inside the mesentery was verified by optical transmission imaging [Fig. 5(c)], while the presence of the CNTs in these cells was manifested by a significantly higher intensity of the 1568-cm^{-1} G peak (106 counts; acquisition time of 0.5 s) above the mesentery tissue background [Fig. 5(d)]. Finally, the consecutive Raman measurements at a 1-s time interval provided simultaneous detection and identification of a single HeLa cell through spatial, temporal, and spectral changes of the Raman signals associated with short periods of time appearance of these cells containing CNTs in the detected volume [Fig. 5(e)]. The clusters of CNTs inside the cells provided significant enhancement of the Raman signals, which increased the RFC capabilities to detect individual HeLa cells in the mesenteric structures.

To further understand the interaction and the developing kinetics of the CNTs after their administration in the lymphatics, Raman mapping analysis was performed by scanning the excitation laser beam across the mesentery tissue (Fig. 6, left) in two directions (*X-Y* mapping) at spatial step sizes of 1 μm of an area situated about 1 cm away from the injection site. The mapping images were built by using Horiba Jobin Yvon LabSpec 5.8 software, based on the *XY* variation of the 1568-cm^{-1} G band intensity. The lighter regions of the Raman images indicated higher concentrations of CNTs while the darker areas represent the lack of or lower concentration of CNTs (Fig. 6, right). The comparison of these 2-D Raman mapping images at 2, 12, 22, and 32 min after the CNT injection and the conventional transmission optical image (Fig. 6, left) indicated a good correlation of the size and shapes of Raman images with the lymphatic vessel size and margins (dashed lines in Fig. 6, right). These results suggest that the CNTs were initially distributed in the broad mesenteric area and then over time became more concentrated in a localized area of lymphatics (bright areas), followed by their further aspiration, collection, and traverse along lymph vessels leading to a decreased CNT concentration in the initial zone (darker spots). In particular, Raman mapping data taken 12 min after the initial injection indicated a very low concentration of CNTs in the interstitial tissue neighboring the lymphatics, while most of the CNT-specific Raman signal was derived preferentially from the lymph vessel. As time progressed further (22 and 32 min postdelivery), the CNTs were transported along the lymph vessels by the lymph flow indicated by an arrow in the optical image, leading to a sequential lower CNT concentration inside the lymphatic area that initially had a high CNT concentration. The Raman mapping data collected for CNTs were compared with the conventional fluorescent dye (FITC) kinetics (Fig. 7), injected intravenously in a rat's tail vein at a concentration that was previously used for fluorescent microscopy[28] and appeared in mesentery lymphatics approximately 1 h after injections. The fluorescent dye was introduced to monitor its kinetics (1 h after injection) into the lymphatic system and to compare its clearance rate with that obtained by Raman mapping for CNTs. The results demonstrate that fast Raman signal acquisition algorithms and their integration into 2-D Raman imaging of tissues by fast *XY* scanning provided a good correlation of the CNTs clearance time with the fluorescent dyes (FITC) when used for the same animal model. Therefore, despite the differences in FITC, CNT properties, and injection procedures, the CNTs were found to present a high mobility and ability to travel through the interstitial tissues, to enter into the lymph system, and to propagate through the lymphatics in a rough analogy to conventional dyes.

4 Discussion

The original experimental data presented in this paper indicate that Raman spectroscopy previously used to mostly study biological systems in stationary conditions *in vivo* or *ex vivo* after

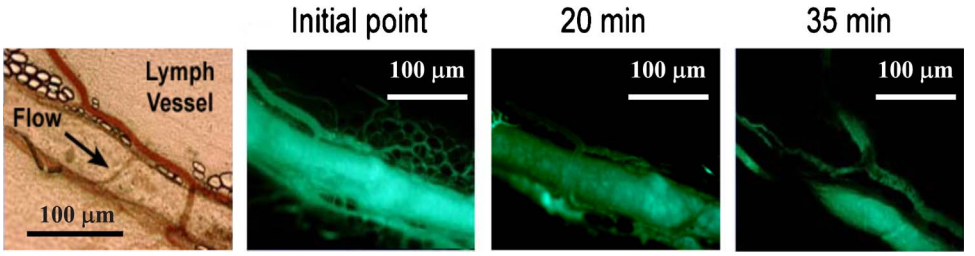

Fig. 7 Fluorescent imaging of dynamic FITC distributions in the mesentery lymphatic.

the animals were sacrificed[24,25] was successfully extended to dynamic *in vivo* studies of biological processes due to the unique properties of CNTs as Raman high-contrast agents and advances in fast Raman signal acquisition. As a result, for the first time, we showed the real-time Raman detection of CNTs in the bloodstream as well as the high ability of CNTs to distribute in tissues and accumulate and further traverse through the lymphatic systems. The distribution rate of CNTs in lymph vessels depends on the activity of these vessels, which in rat mesentery varies between a complete absence of lymph flow, low flow velocity in the range of 0.05 to 0.2 mm/s (as observed for the vessels that were analyzed in this study), and relatively high flow velocity up to 0.5 to 3 mm/s and even more in limited vessels.[28] In addition to lymphatics, time-resolved RFC also demonstrated the capability for real-time detection of CNT pharmokinetics *in vivo* in the blood circulation with relatively high flow velocity values[28] of 3 to 5 mm/s. The travel time of individual CNTs through the detected volume under the parameters of our experiments was estimated to be around 3 to 5 ms, which is close to the temporal resolution of current RFC schematics (~7 ms). This makes it difficult to detect individual nanoparticles in fast blood flow. However, the current RFC schematic enables studying the CNT clearance rate when many nanoparticles are present in the bloodstream. According to our estimation, RFC, with the current threshold sensitivity, can be used for real-time monitoring of circulating CNTs with simultaneous presence of at least 60 individual CNTs (or their small clusters) in the laser focal volume. Nevertheless, this rough quantitative estimate requires further verifications. Further improvement may include new schematics for detection of flash Raman signals in the presence of a relatively stable background from tissue and blood, the use of optimized spectral range, linear laser beam geometry, and advancing the signal acquisition algorithm, which could approach the sensitivity detection threshold to a few individual CNTs in the detected volume.

The similar clearance kinetics obtained for CNTs and FITC may indicate that the behavior of the CNTs in various biological systems is likely driven by their small diameters rather than lengths, a fact which should indicate a "snaking" effect during their distribution and travel in blood, lymph, or other tissues. When CNTs penetrate and accumulate into cancer cells and assemble into clusters, a significant Raman signal enhancement provides the capabilities for *in vivo* detection of single cancer cells with their identification based on the specific spectral fingerprint of CNTs. Thus, this *in vivo* Raman flow cytometry technique can be considered as a new tool in biological research with many potential applications, including the study of CNT pharmokinetics; visualization of lymphatics including lymph nodes (Raman lymphography); selective detection of circulating cancer cells, bacteria, or other biological systems targeted by CNTs, possibly functionalized with antibodies, DNA, or folates.[1,4,19] The current schematic enables us to assess superficial microvessels with depth up to few (1 to 3) millimeters, which may be quite enough for many mentioned applications. Nevertheless, the use of the NIR spectral range and high contrast Raman agents[26] (e.g., SERS tags) may further improve these parameters up to 1 to 2 cm.

The potential advantages of RFC with CNTs as contrast agents, compared to radioactive or fluorescent probes, is related to the relatively lower toxicity, rapid spectral CNT identification, and the selective targeting of cancer cells or infections. Nevertheless, additional studies are required to fully understand the potential toxic effects of the CNTs before their use in humans. Compared to the PA technique,[17–19] RFC may provide high specificity of the corresponding scattering molecular spectra, which can be collected during cell movement through the detected volume. For spectral identification, the PA technique requires several laser wavelengths,[18] while Raman spectroscopy may operate with just one wavelength. Fluorescent measurements in flow cytometry are limited by the broad emission spectra of fluorescent labels.[26] By contrast, Raman spectra exhibit relatively narrow spectral futures, and contain information on the chemical composition of the samples. On the other hand, the ability of CNTs to provide both strong Raman, fluorescent, PT and PA signals,[1,3,10,12,17–19] enables the possible integration of all these methods in one technical flow cytometry platform that could become universally applicable to objects with various absorption, fluorescent, and Raman scattering properties. In particular, the label-free nature of Raman and PT/PA spectroscopy using intrinsic cell molecular markers provides opportunities for *in vivo* non-invasive blood and lymph biochemistry analysis. The integration of RFC-based nanodiagnostics with PT molecular therapy and a NIR laser[1–3] may provide RFC-guided selective nanophotothermolysis[3] with CNTs for treatment of lymphatic diseases, metastases (e.g. in the sentinel lymph nodes), circulating individual metastatic cells, or inhibition of pathological lymphatic networks around primary tumors to prevent the occurrence of metastasis.

Acknowledgments

This work was supported add by the National Institute of Health under Grant Nos. EB000873 and EB005123, and CA131164, by the Arkansas Bioscience Institute, and by Arkansas Science and Technology Authority (ASTA) under Grant No. 08-CAT-03.

References

1. N. W. S. Kam, M. O'Connell, J. A. Wisdom, and H. Dai, "Carbon nanotubes as multifunctional biological transporters and near-infrared agents for selective cancer cell destruction," *Proc. Natl. Acad. Sci. U.S.A.* **102**, 11600–11605 (2005).
2. V. P. Zharov, J.-W. Kim, D. T. Curiel, and M. Everts, "Self-assembling nanoclusters in living systems: application for integrated photothermal nanodiagnostics and nanotherapy," *Nanomedicine* **1**, 326–345 (2005).
3. J.-W. Kim, E. I. Galanzha, E. V. Shashkov, N. Kotagiri, and V. P. Zharov, "Photothermal antimicrobial nanotherapy and nanodiagnostics with self-assembling carbon nanotube clusters," *Lasers Surg. Med.* **39**, 622–634 (2007).
4. M. Shim, N. W. S. Kam, R. J. Chen, Y. Li, and H. Dai, "Functionalization of carbon nanotubes for biocompatibility and biomolecular recognition," *Nano Lett.* **2**, 285–288 (2002).
5. J. A. Rojas-Chapana, J. Troszcynska, I. Firkowska, C. Morsczeck, and M. Giersig, "Multi-walled carbon nanotubes for plasmid delivery into *Escherichia coli* cells," *Lab Chip* **5**, 536–539 (2005).
6. M. L. Becker, J. A. Fagan, N. D. Gallant, B. J. Bauer, V. Bajpai, E. K. Hobbie, S. H. Lacerda, K. B. Migler, and J. P. Jakupciak, "Length-dependent uptake of DNA-wrapped single-walled carbon nanotubes," *Adv. Mater. Res.* **19**, 939–945 (2007).

7. Z. Liu, M. Winters, M. Holodniy, and H. Dai, "siRNA delivery into human, T. cells and primary cells with carbon nanotube transporters," *Angew. Chem., Int. Ed.* **46**, 2023–2027 (2007).
8. A. Bianco, K. Kostarelos, C. D. Partidos, and M. Prato, "Biomedical applications of functionalized carbon nanotubes," *Chem. Commun. (Cambridge)* 571–577 (2005).
9. N. W. S. Kam, T. C. Jessop, P. A. Wender, and H. N. Dai., "Nanotube molecular transporters: internalization of carbon nanotube-protein conjugates into mammalian cells," *J. Am. Chem. Soc.* **126**, 6850–6851 (2004).
10. P. Cerukuri, S. M. Bachilo, S. H. Litovsky, and R. B. Weisman, "Near-infrared fluorescence microscopy of single-walled carbon nanotubes in phagocytic cells," *J. Am. Chem. Soc.* **126**, 15638–15639 (2004).
11. D. Pantarotto, J.-P. Briand, M. Prato, and A. Bianco, "Translocation of bioactive peptides across cell membrane by carbon nanotubes," *Chem. Commun. (Cambridge)* 16–17 (2004).
12. T. K. Leeuw, R. M. Reith, R. A. Simonette, M. E. Harden, P. Cherukuri, D. A. Tsyboulski, K. M. Beckingham, and R. B. Weisman, "Singlewalled carbon nanotubes in the intact organism: near-IR imaging and biocompatibility studies in *Drosophilia*," *Nano Lett.* **7**(9), 2650–2654 (2007).
13. R. Singh, D. Pantarotto, L. Lacerda, G. Pastorin, C. Klumpp, M. Prato, A. Bianco, and K. Kostarelos, "Tissue biodistribution and blood clearance rates of intravenously administered carbon nanotube radiotracers," *Proc. Natl. Acad. Sci. U.S.A.* **103**(9), 3357–3762 (2006).
14. P. Cherukuri, C. J. Gannon, T. K. Leeuw, H. K. Schmidt, R. E. Smalley, S. A. Curley, and R. B. Weisman, "Mammalian pharmacokinetics of carbon nanotubes using intrinsic nearinfrared fluorescence," *Proc. Natl. Acad. Sci. U.S.A.* **103**, 18882–18886 (2006).
15. N. L. Mills, N. Amin, S. D. Robinson, A. Anand, J. Davies, D. Patel, J. M. de la Fuente, F. R. Cassee, N. A. Boon, W. MacNee, A. M. Millar, K. Donaldson, and D. E. Newby, "Do inhaled carbon nanoparticles translocate directly into the circulation in humans?" *Am. J. Respir. Crit. Care Med.* **173**, 426–431(2006).
16. J. Guo, X. Zhang, and W. Li., "Biodistribution of functionalized multiwall carbon nanotubes in mice," *Nucl. Med. Biol.* **34**, 579–583 (2007).
17. V. P. Zharov, E. I. Galanzha, E. V. Shashkov, J.-W. Kim, N. G. Khlebtsov, and V. V. Tuchin, "Photoacoustic flow cytometry: principle and application for real-time detection of circulating single nanoparticles, pathogens, and contrast dyes *in vivo*," *J. Biomed. Opt.* **12**, 0551503 (2007).
18. E. I. Galanzha, E. V. Shashkov, V. V. Tuchin, and V. P. Zharov, "In vivo multispectral multiparameter photoacoustic lymph flow cytometry with natural cell focusing, label-free detection and multicolor nanoparticle probes," *Cytometry, Part A* **73A**, 884–894 (2008).
19. A. De la Zerda, C. Zavaleta, S. Keren, S. Vaithilingam, S. Bodapati, Z. Liu, J. Levi, B. R. Smith, T. J. Ma, O. Oralkan, Z. Cheng, X. Chen, H. Dai, B. T. Khuri-Yakub, and S. S. Gambhir "Carbon nanotubes as photoacoustic molecular imaging agents in living mice," *Nat. Nanotechnol.* **3**, 557–562 (2008).
20. J. T. Motz, S. J. Gandhi, O. R. Scepanovic, A. S. Haka, J. R. Kramer, R. R. Dasari, and M. S. Feld, "Real-time Raman system for in vivo disease diagnosis," *J. Biomed. Opt.* **10**, 031113 (2005).
21. M. S. Dresselhaus, G. Dresselhaus, R. Saito, and A. Jorio, "Raman spectroscopy of carbon nanotubes," *Phys. Rep.* **409**, 47–99 (2005).
22. M. S. Dresselhaus, G. Dresselhaus, A. Jorio, A. G. Souza Filho, and R. Saito, "Raman spectroscopy on isolated single wall carbon nanotubes" *Carbon* **40**, 2043–2061 (2002).
23. A. Jorio, M. A. Pimenta, A. G. Souza Filho, R. Saito, G. Dresselhaus, and M. S. Dresselhaus, "Characterizing carbon nanotube samples with resonance Raman scattering," *New J. Phys.* **5**, 139.1–139.17 (2003).
24. X. Qian, X.-H. Peng, D. O. Ansari, Q. Yin-Goen, G. Z. Chen, D. M. Shin, L. Yang, A. N. Young, M. D. Wang, and S. Nie, "In vivo tumor targeting and spectroscopic detection with surface enhanced Raman nanoparticle tags," *Nat. Biotechnol.* **26**, 83–90 (2007).
25. Z. Liu, C. Davis, W. Cai, L. He, X. Chen, and H. Dai, "Circulation and long-term fate of functionalized, biocompatible single-walled carbon nanotubes in mice probed by Raman spectroscopy," *Proc. Natl. Acad. Sci. U.S.A.* **105**, 1410–1415 (2008).
26. D. A. Watson, L. O. Brown, D. F. Gaskill, M. Naivar, S. W. Graves, S. K. Doorn, and J. P. Nolan,"A flow cytometer for the measurement of Raman spectra," *Cytometry, Part A* **73**(2),119–28 (2008).
27. A. R. Biris, Z. Li, E. Dervishi, D. Lupu, Y. Xu, V. Saini, F. Watanabe, and A. S. Biris, "Effect of hydrogen on the growth and morphology of single wall carbon nanotubes synthesized on a Fe–Mo/MgO catalytic system," *Phys. Lett. A* **372**, 3051–3057 (2008).
28. E. I. Galanzha, V. V. Tuchin, and V. P. Zharov, "Advances in small animal mesentery models for *in vivo* flow cytometry, dynamic microscopy, and drug screening (review)," *World J. Gastroenterol.* **13**, 192–218 (2007).